ISSN 1061-8309, Russian Journal of Nondestructive Testing, 2020, Vol. 56, No. 12, pp. 960–970. © Pleiades Publishing, Ltd., 2020.
Russian Text © The Author(s), 2020, published in Defektoskopiya, 2020, No. 12, pp. 14–23.

ACOUSTIC METHODS

Monitoring Composite Fiber Failure Using Acoustic Emission System, Vibration Analyzer, and High-Speed Video Recording

N. A. Makhutov[a], V. I. Ivanov[b], A. G. Sokolova[a], I. E. Vasil'ev[a, *], D. V. Chernov[a], D. F. Skvortsov[a], and M. A. Bubnov[a]

[a] *Mechanical Engineering Research Institute, Russian Academy of Sciences, Moscow, 101990 Russia*

[b] *ZAO RII MSIA "Spectrum", Moscow, 119048 Russia*

**e-mail: vie01@rambler.ru*

Received August 27, 2020; revised October 7, 2020; accepted October 9, 2020

Abstract—We consider the nature of the phenomenon of acoustic emission (AE) occurring in the process of deformation and destruction of solid bodies. A theoretical analysis of the processes of transformation and dissipation of energy during the destruction of structural bonds of an idealized model of a solid has been carried out. Using A-line32D and PCI-2 AE systems, Onyx vibration analyzer, and Videosprint high-speed camera, as well as numerical simulation in the LS-DYNA software environment, we study wave processes occurring during deformation and rupture of reinforcing fibers of composite materials. The obtained experimental and calculation data indicate that the main energy is emitted within the period of the aftereffect of fiber rupture in the range of sound frequencies less than 2 kHz. In this case, the energy of the peak values recorded in the ultrasonic frequency range does not exceed several percent of the maximum level at the carrier frequency in the audio range.

Keywords: acoustic emission, video recording, vibration analyzer, destruction of materials, fiber break, signal amplitude, energy, frequency spectrum

DOI: 10.1134/S1061830920120049

INTRODUCTION

The movement of dislocations, the formation of cracks in the crystal lattice of a metal, or the destruction of structural bonds in a polymer composite material (PCM) causes irreversible displacements of neighboring bonds, accompanied by a change in the stress-strain state both in the zone of structural damage and in the adjacent region of the structure [1, 2].

Irreversible displacements occurring at the moments of plastic deformation or destruction of structural bonds propagate in a solid body in the form of elastic waves of discrete or continuous ultrasonic pulses. Acoustic emission (AE) transducers are used to record the pulses and convert them into electrical signals. In this case, the transducer records AE pulses if

• nonlinear (irreversible) displacements occur in the material of a solid during its deformation (this is a necessary condition);

• medium displacement pulses are generated in the ultrasonic frequency range at $f \geq 20$ kHz with an amplitude exceeding the level of a signal discrimination threshold in the passband of digital filters in the recording equipment (this is a sufficient condition).

THEORETICAL JUSTIFICATION

Irreversible displacements of structural bonds (u_i) resulting from plastic deformation and violation of continuity of solid bodies generate elastic waves in a wide frequency range from several hertz to several megahertz [1–3],

$$u(r,t) = u_0 + \sum_{k=1}^{k=n} a(k)\exp[i(kr - \omega(k)t)], \quad (1)$$

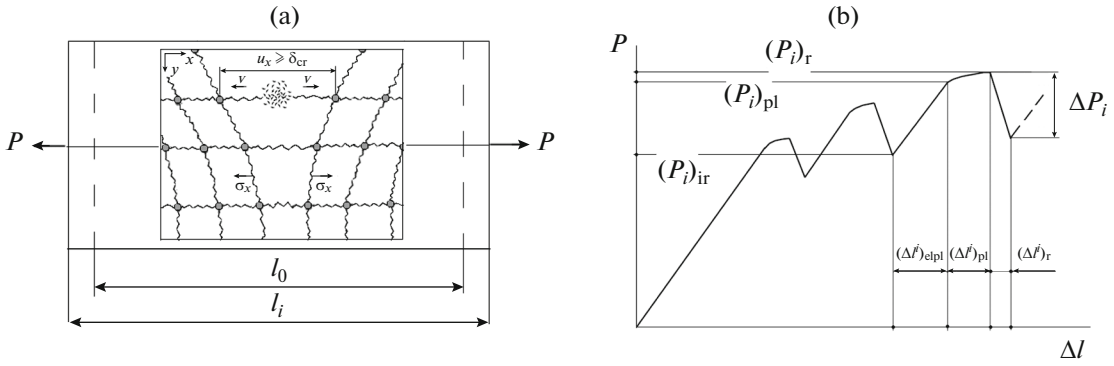

Fig. 1. Scheme of destruction of a structural bond in the solid body model (a) and diagram of its uniaxial tension (b) in P–Δt coordinates.

where $r=\{x,y,z\}$ is the radius vector; t is time; $a(k)$ are the amplitudes of wave modes; $k = 2\cdot\pi / \lambda$ is the wave vector; λ is the wavelength; $\omega(k) = 2\pi f$ is the angular frequency (rad/s); f is frequency in Hz; $v_{ph}=\omega(k)k$ is the phase velocity of the kth mode; $\exp[i(kr-\omega(k)t)] = e^{i(kr-\omega(k)t)} = \cos(kr - \omega(k)t) + i\cdot\sin(kr - \omega(k)t)$, and u_0 is the initial displacement.

The potential energy (Π_{el}^r) released upon destruction of a structural bond is equal to the work (A) of overcoming the elastic resistance forces during deformation of the material from the initial equilibrium state (ε_0) to the limit state (ε_v) in which destruction has occurred less the energy spent on plastic deformation and destruction ($\varepsilon_v - \varepsilon_{pl}$):

$$\Pi_{el}^r = A - \Pi_{pl}^d = \int_{l_i}^{l_{i+1}} P(l)dl - \int_{\varepsilon_{pl}}^{\varepsilon_v} \sigma(\varepsilon)d\varepsilon. \quad (2)$$

To consider the processes of transformation and dissipation of energy emitted at the moment of destruction of a structural bond, we represent a solid in the form of a flat model whose structure is a uniformly distributed system of spherical elements interconnected by elastic bonds. This model is schematically depicted in Fig. 1a.

When loading an ideal rigid body with a tensile force, we consider the process of destruction of an elastic bond and the energy released in this case. The diagram in Fig. 1b, presented in the P–Δl coordinates (load–specimen elongation increment), shows the jumps on the loading curve that occur during deformation and destruction of structural bonds. When an elastic bond is destroyed, the rigidity of the system decreases ($E\cdot F$, where E is the elastic modulus and F is the cross-sectional area at the point of bond failure) and its compliance ($C = \Delta l/P$) increases. This is reflected in the loading diagram by a drop in load by ΔP_i and an increment in linear elongation by Δl_i. In this case, the potential energy of elastic deformation released during the breakage of the ith bond is

$$(\Pi_{el}^r)_i = (\Delta P_i \times \Delta l_i)/2. \quad (3)$$

The potential energy released when a structural bond is dissipated through the movement of particles of the broken material volume, the elastic contraction of the elements of neighboring links, and internal friction—the resistance of the medium to the free movement of the broken bond elements.

Figure 2 presents a diagram of the transformation of the released elastic deformation energy Π_r accompanied by its dissipation, during the aftereffect of the rupture of a structural bond in a solid body.

The moments t_r, t_m, and t_{cmp} are marked on the timeline. These moments correspond to the maximum fiber tension u_r^{max}, the equilibrium state $u_m = 0$, in which the velocities of the particles and the contraction of the elements of the broken bond reach their maximum values (v_{ir}^{max}, v_r^{max}), and the largest displacement of neighboring links u_{cmp}^{max} due to the action of inertial compression forces.

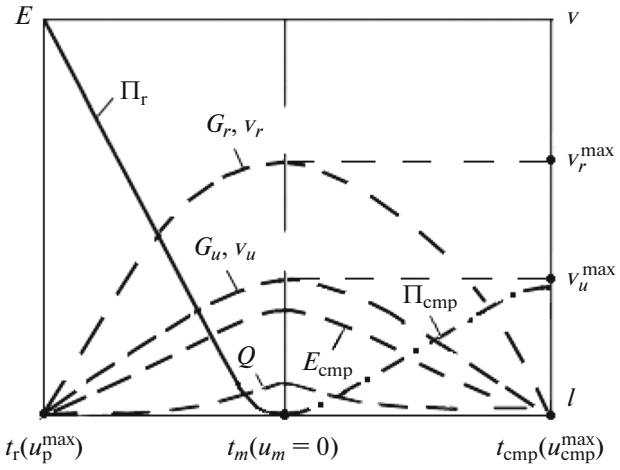

Fig. 2. Diagram of transformation of elastic deformation energy (Π_r) during the period $t_r - t_{cmp}$ of aftereffect of structural bond rupture; v_u and v_r are the speeds of motion of particles and of contraction of elements of broken bond.

As follows from the diagram in Fig. 2, the process of transformation and dissipation of elastic energy released by the broken bond can be divided into two characteristic periods. During the period $t_r - t_m$, the potential energy of elastic deformation (Π_r) is transformed into the energy of contraction of the stretched adjacent links (G_r) and the kinetic energy of motion of particles of the destroyed material volume (G_u), which dissipates due to the impact action and emergence of bulk compression waves (E_{cmp}) in a solid body, as well as the release of thermal energy (Q) caused by the internal friction occurring when the elements of the broken bond are displaced,

$$\Pi_r \rightarrow G_r + G_{ir} - (C_{cmp} + Q). \tag{4}$$

During the period $t_m - t_{cmp}$, the kinetic energy of the inertial motion of the broken bond elements is converted into the potential compression energy (Π_{cmp}), the impact energy (E_{cmp}), and the generation of heat (Q) due to internal friction,

$$G_r + G_u \rightarrow \Pi_{cmp} + E_{cmp} + Q. \tag{5}$$

Ultimately, the main energy of elastic deformation of the broken bond is transformed into the kinetic (K) and potential (Π) energy of the wave processes causing the generation of displacement pulses of the medium in a wide range of frequencies, including the ultrasonic range, that is, the emergence of AE signals,

$$K = \frac{\rho}{2}\sum_{k=1}^{k=n} a^2(k)\omega^2(k)\sin^2(kx - \omega(k)t), \tag{6}$$

$$\Pi = \frac{E}{2}\sum_{k=1}^{k=n} a^2(k)k^2\cos^2(kx - \omega(k)t). \tag{7}$$

In this case, if the total energy of elastic waves generated as a result of the structural bond rupture and the work (A) done by external forces at the tip of the growing crack exceeds the energy G_γ required to overcome the resistance of cohesive and adhesive forces fastening structural bonds at the tip of the growing crack, then the conditions necessary for the formation of a new fracture surface emerge,

$$A + K + \Pi \geq G_\gamma. \tag{8}$$

The crack initiation and formation of a new surface occurs if the opening of the crack edges (δ_i) at its tip exceeds the limit level (δ_{cr}). This is a sufficient condition [3–6],

$$\delta_i \geq \delta_{cr}. \tag{9}$$

The propagation of the crack is accompanied by the destruction of new structural bonds, and, consequently, by a chain reaction in which the released energy is converting into elastic waves of displacement

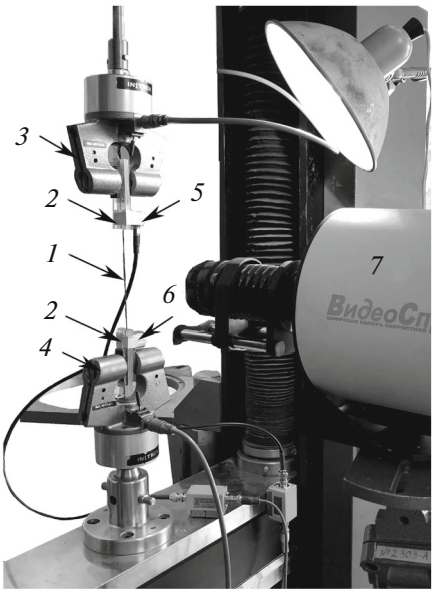

Fig. 3. Tensile tests of Kevlar sample with Instron-1195 unit: (*1*) carbon fiber, (*2*) Plexiglass® plates, (*3* and *4*) pneumatic grippers, (*5* and *6*) AE transducers, (*7*) Videosprint camera.

of neighboring links. This causes the material at the crack tip to deform and further advance of the crack as long as the necessary (8) and sufficient conditions (9) for its growth are fulfilled. Local microfracture of the structural material occurs in the area adjacent to the crack tip in the zone of maximum deformations, and a crack jump is the result of the fusion of the new surface, formed during the destruction of the structural bond, with the enlarged crack. At the moment of crack growth in the area adjacent to the newly formed crack surface, an instantaneous change in stresses occurs, accompanied by the emission of elastic waves.

A high stress gradient in the area of the stress raisers, where the material structure usually has an increased defectiveness due to technological operations at the stages of product manufacturing, contributes to the intensive accumulation of damage. Therefore, violations of structural bonds in the form of breaks, formation and annihilation of dislocations in the crystal lattice of metals, and the initiation and development of cracks in composite structures can occur in the zones of developing defects and damages located in the area of technological stress raisers (welds, cutouts, holes, etc.), as early as at the initial stage of loading under conditions of elastic deformation of the product's main material.

The greater the stiffness of the broken structural bond, determined by the elastic modulus, the area, and the moment of inertia, the greater the energy released during the destruction of this bond. For example, AE signals are not recorded in acoustically inert polymer materials such as Plexiglass®, which have an elastic modulus more than two orders of magnitude smaller than CFRPs, during their plastic deformation. This is explained by the low amplitude of the generated pulses, which is at or below the hardware noise level in the recording equipment. When testing products made of polymer composite materials, AE pulses begin to be recorded at the early stages of loading under conditions of elastic deformation, which is due to the high fragility of the structural elements of the matrix, the difference in the physicomechanical characteristics of the binder and reinforcing fibers, and the different directions of fiber layout in the layers of PCM pack, i.e., due to the anisotropy in properties.

STUDYING WAVE PROCESSES DURING FIBER RUPTURE

Experimental studies of wave processes occurring during deformation and destruction of the structure of solid bodies were carried out during the rupture of reinforcing fibers of composite materials. Tests on the rupture of samples of carbon fiber, Kevlar, and boron fiber were carried out with an Instron-1195 testing machine. The processes were recorded using a high-speed VideoSprint (OOO "UVN Technologii") camera working concurrently with A-line32D (Interunis-IT LLC) and PCI-2 (Mistras, USA) acoustic emission systems. Figure 3 shows a sample of Kevlar fiber (*1*) in the grips (*3* and *4*) of the loading stand. To reduce mechanical noise due to the grips, the AE transducers (*5* and *6*) were mounted on Plexiglas® plates (*2*) (AE-inert material) between which the investigated fiber (*1*) was clamped. The plates (*2*) were

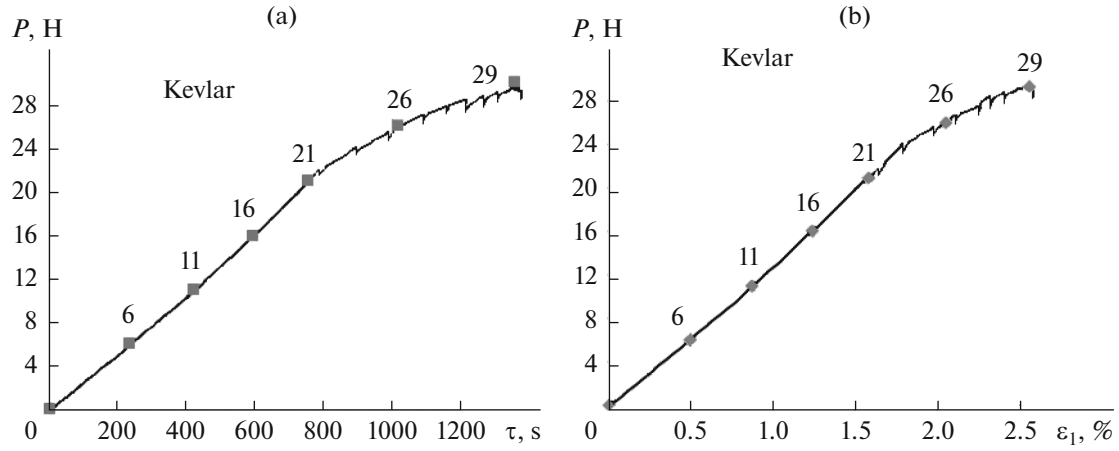

Fig. 4. Kevlar loading diagrams in P is the τ coordinates (a) and P is the ε_1 coordinates (b).

clamped in pneumatic grippers (*3* and *4*) of the lower and upper traverses of the stand. The fiber was loaded automatically at a speed of 1 mm/min. To record AE events with the A-line32D system, we used SNK-06 (OOO "Strategiya NK") bandpass transducers with a resonance frequency of 60 kHz, while for the four-channel PCI-2 system, we used the low-frequency R6I-AST (Mistras, USA) integrated transducers with a resonance frequency of 55 kHz. To amplify the signals recorded by these transducers, PAEF-014 (Interunis-IT LLC) and 2-4-6-AST (Mistras, USA) were used.

Loading diagrams of the Kevlar fiber sample plotted in load–time and load–strain coordinates are shown in the graphs in Figs. 4a and 4b, respectively.

Figure 5 shows the results of recording of AE events by the acoustic emission transducers (AETs) that were linearly locating the process of continuous deformation of the Kevlar fiber until its destruction, which occurred at 1344 s of testing at the strain of $\varepsilon_1 = 2.62\%$ and the tensile load level of $P_B = 29.1$ N.

As follows from the graph in Fig. 5a, the accumulation of AE events occurred most intensively at a distance of 45 mm from AET no. 1, where the stretched 80-μm–diameter Kevlar fiber clamped in the Plexiglass® plates at a distance of 110 mm between the AE transducers broke at the 1344 s of loading. The scatter of AE event indication locations observed in the graph in Fig. 5a indicates that, as the fiber was stretched, the destruction of individual filaments (fibrils) was recorded within the interval $\Delta X = \pm 15$ mm relative to the place of the forthcoming rupture. A total of 120 AE events were recorded during fiber tensile testing. Moreover, as can be seen from the graph in Fig. 5b, half of them were recorded during the last 60 s of testing. As follows from the graph in Fig. 5c, the maximum amplitudes of location pulses, reaching 90–100 dB, caused by the massive rupture of filaments were recorded with the load increased to 25–29 N and with the strain level of $\varepsilon_1 = 2.0$–2.6% during 1100–1344 s of loading.

Figure 6 shows the shapes and spectra of AE pulses recorded by the SNK-06 (a, b) and R6I-AST (c, d) transducers using the A-line32D and PCI-2 systems at the time of the breakage of the Kevlar fiber. It can be seen from the signal spectra shown in the graphs in Figs. 6b and 6d that the maximum energy during the breakage of the Kevlar fiber was recorded in the low-frequency range of ultrasonic waves for $f = 25$–30 kHz (much lower than the resonance frequencies of the used AE transducers, which are 60 and 55 kHz for the SNK-06 and R6I-AST, respectively).

Figure 7 shows the pictures of the rupture of a bundle of carbon fiber and Kevlar, recorded using the high-speed Videosprint video camera at a shooting speed of 1000 frames per second. When the reinforcing fibers break in the structure of the PCM pack, the energy of motion of destroyed material particles and of the contraction of structural bonds is transformed into elastic waves of medium displacement pulses, which cause vibration effects in the entire product. Moreover, the most affected are the neighboring bonds, in which the main energy of the generated pulses is absorbed.

AE pulses that occur as a result of the dynamic restructuring of the structural bonds in the deformed material are recorded by the AE equipment immediately upon occurrence of irreversible displacements in the medium. The wave processes associated with the impact of material particles of the broken bond, the contraction of deformed elements, and the release of heat, already result from the aftereffect of the structural bond breakage. The delay of the active phase of the wave processes relative to the time of the breakage

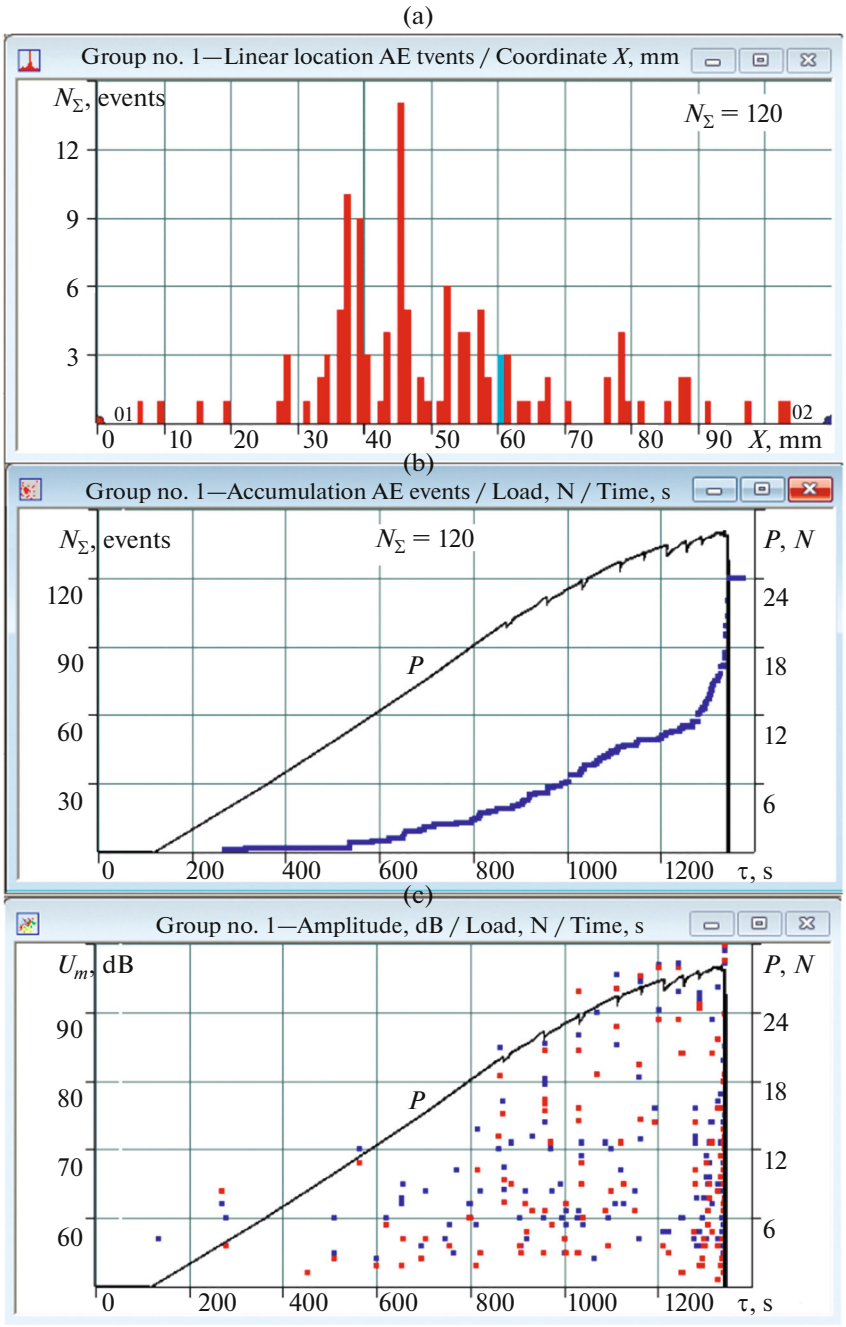

Fig. 5. Results of AE monitoring of Kevlar fiber under tension recorded at 1344 s of testing at strain value $\varepsilon_1 = 2.62\%$ and tensile load level $P_B = 29.1$ N.

itself is milliseconds. To record low-frequency pulses in the range from 1 to 50 kHz, arising as the fiber breakage aftereffect, experimental studies were carried out using the Oniks (Diamech-2000 Ltd., Russia) vibration analyzer. An AC102 accelerometer and a Z-501 microphone were used as receivers of low-frequency vibrations arising under medium disturbances. The loading diagram of the Kevlar fiber during tensile tests is shown in Fig. 8.

To determine the carrier frequency of the maximum energy release during the aftereffect of the Kevlar fiber breakage, we numerically simulated this process in the LS-DYNA software environment [6]. In the calculations, we used an elastoplastic formulation with a deformation criterion of fracture [3], implemented for a piecewise linear plasticity type material model [6]. The scheme of integration over time was used with static preloading of the thread by tensile stresses close to the Kevlar yield point $\sigma_{02} = 3$ GPa [7].

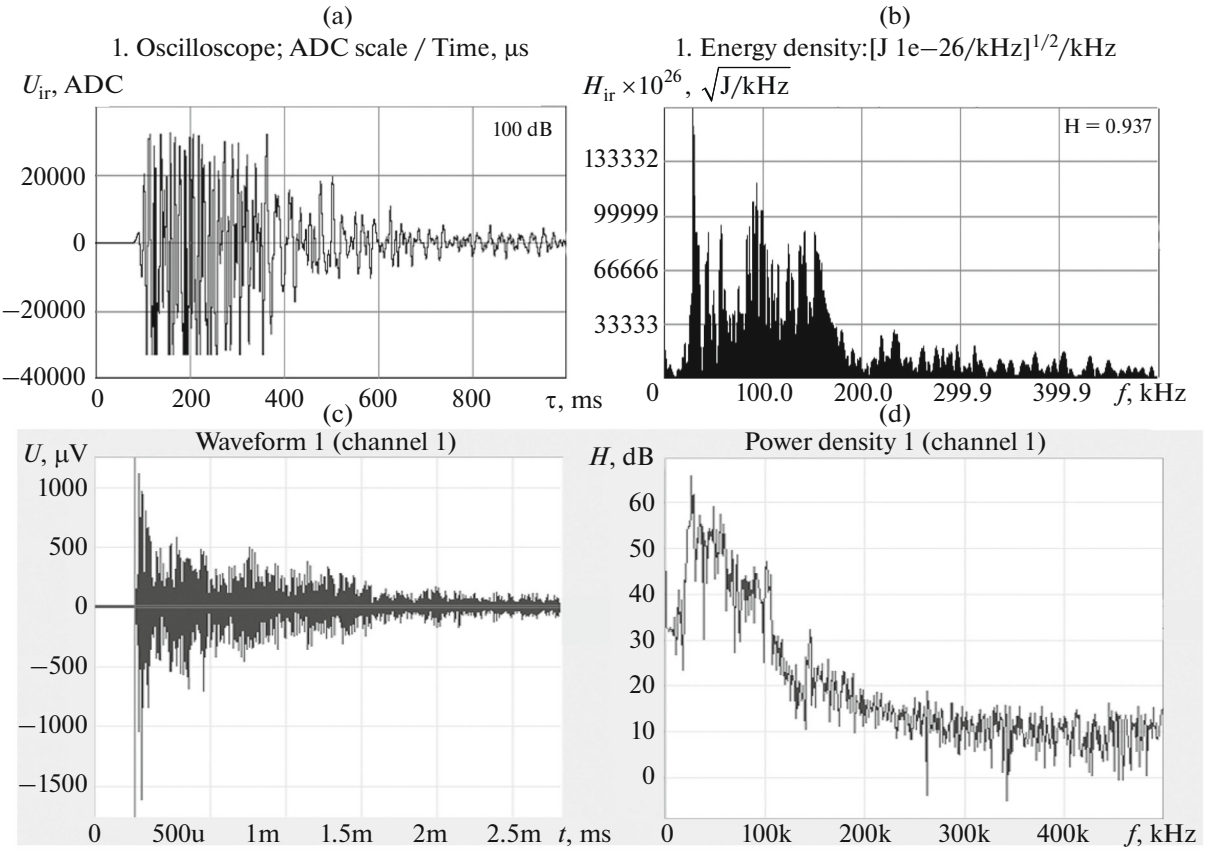

Fig. 6. Waveforms (a, c) and spectra (b, d) of AE pulses recorded at the moment of rupture of Kevlar fiber using SNK-06 (a, b) and R6I–AST (c, d) transducers.

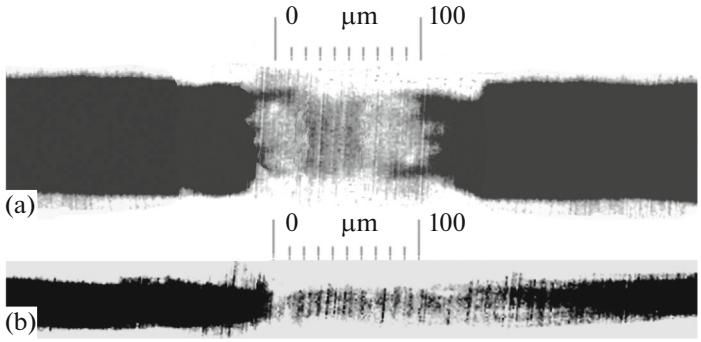

Fig. 7. Moments of rupture a bundle of carbon fiber (a) and Kevlar (b) recorded with high-speed Videosprint camera at a shooting speed of 1000 frames per second.

Figure 9 shows the finite-element model of the deformed state of the left-hand side of the Kevlar fiber at the moment of rupture, corresponding to the high-speed video frame shown in Fig. 7b.

Since the pulse energy is proportional to the square of the recorded parameter amplitude, in order to obtain the relative density of amplitude distribution in the frequency range of the transducers employed, the amplitude values of the parameters were squared and divided by the maximum value of the amplitude,

$$\chi = \frac{A_i^2(f)}{A_{\max}^2} \times 100\%. \quad (10)$$

Figure 10 shows the waveforms and spectra of the relative energy density (χ) calculated on the basis of experimental data recorded by the accelerometer (a) and the microphone (c). The recorded data are compared with the graphs of the design values (d, f) obtained by numerical simulation.

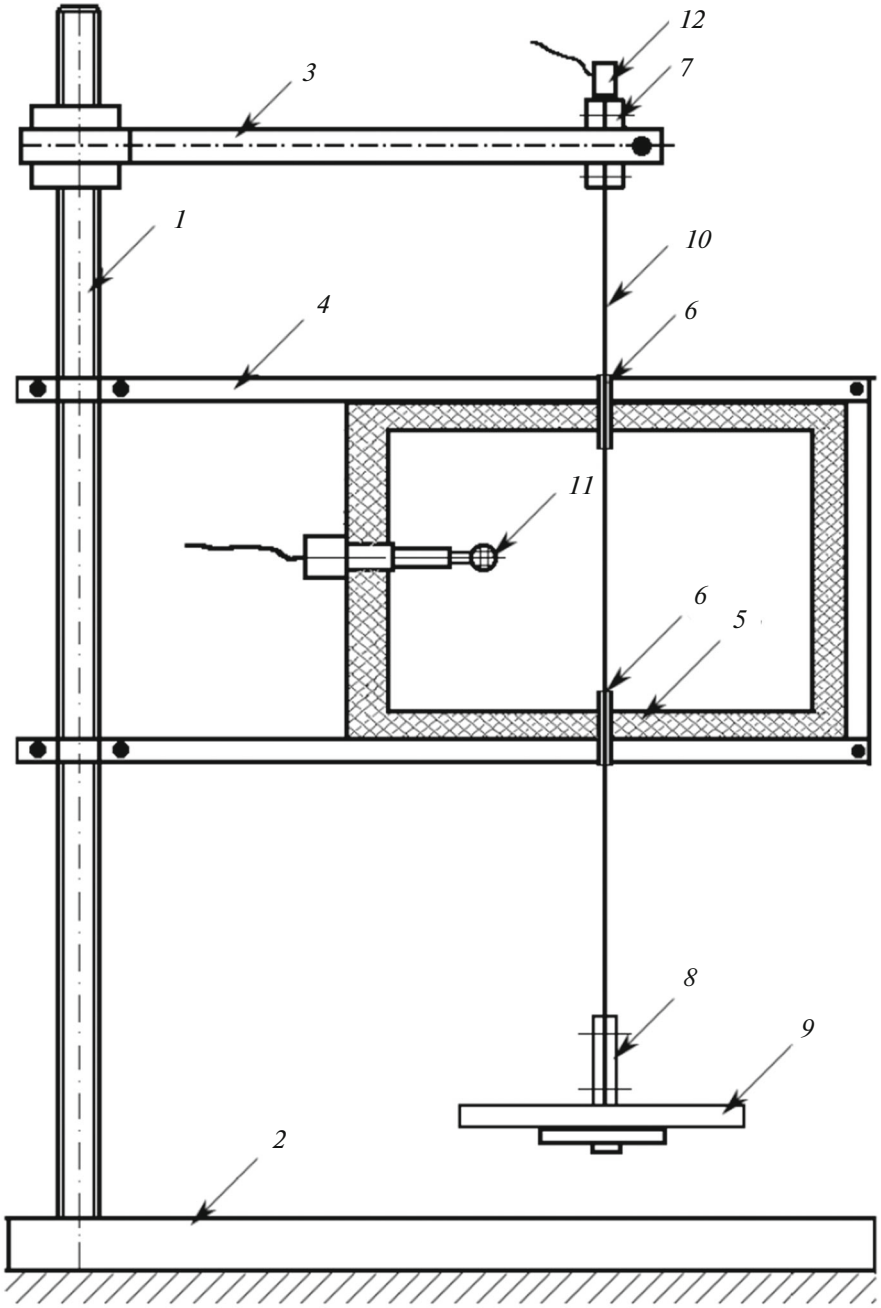

Fig. 8. Loading device diagram for tensile testing of Kevlar fibers: (*1*) vertical rack, (*2*) tripod base, (*3*) power arm, (*4*) acoustic chamber bracket arm, (*5*) acoustic chamber, (*6*) polymer guide tube, (*7*) upper magnetic fiber clamp, (*8*) lower fiber clamp with suspension, (*9*) calibrated weights, (*10*) stretched fiber, (*11*) microphone, (*12*) acceleration sensor (accelerometer).

As follows from the spectra of these graphs constructed on the basis of experimental data and obtained as a result of numerical simulation, the maximum energy of pulses arising during the aftereffect of a fiber breakage is released in the region of sound frequencies of $f < 2$ kHz. The energy spectra of these processes differ significantly from those shown in the graphs in Fig. 6, recorded by the R15α-AST and R6I-AST transducers at the time moment of Kevlar fiber breakage.

Individual peak values of the energy release density in the frequency range $f = 2–20$ kHz can be noted in the spectra in Figs. 10b and 10d. Some maxima were also recorded in the ultrasonic frequency range at $f > 20$ kHz. The discrepancy between the peak frequencies of the maximum energy release in the audio

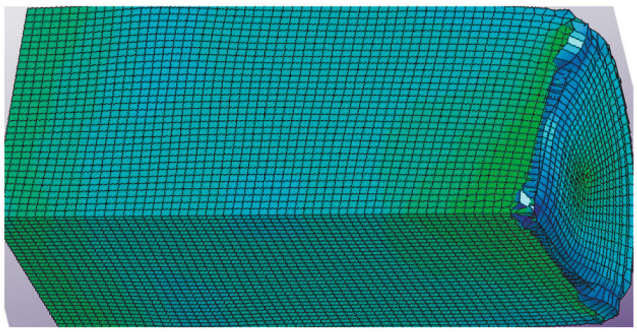

Fig. 9. Numerical simulation of Kevlar fiber breakage in LS-DYNA software environment.

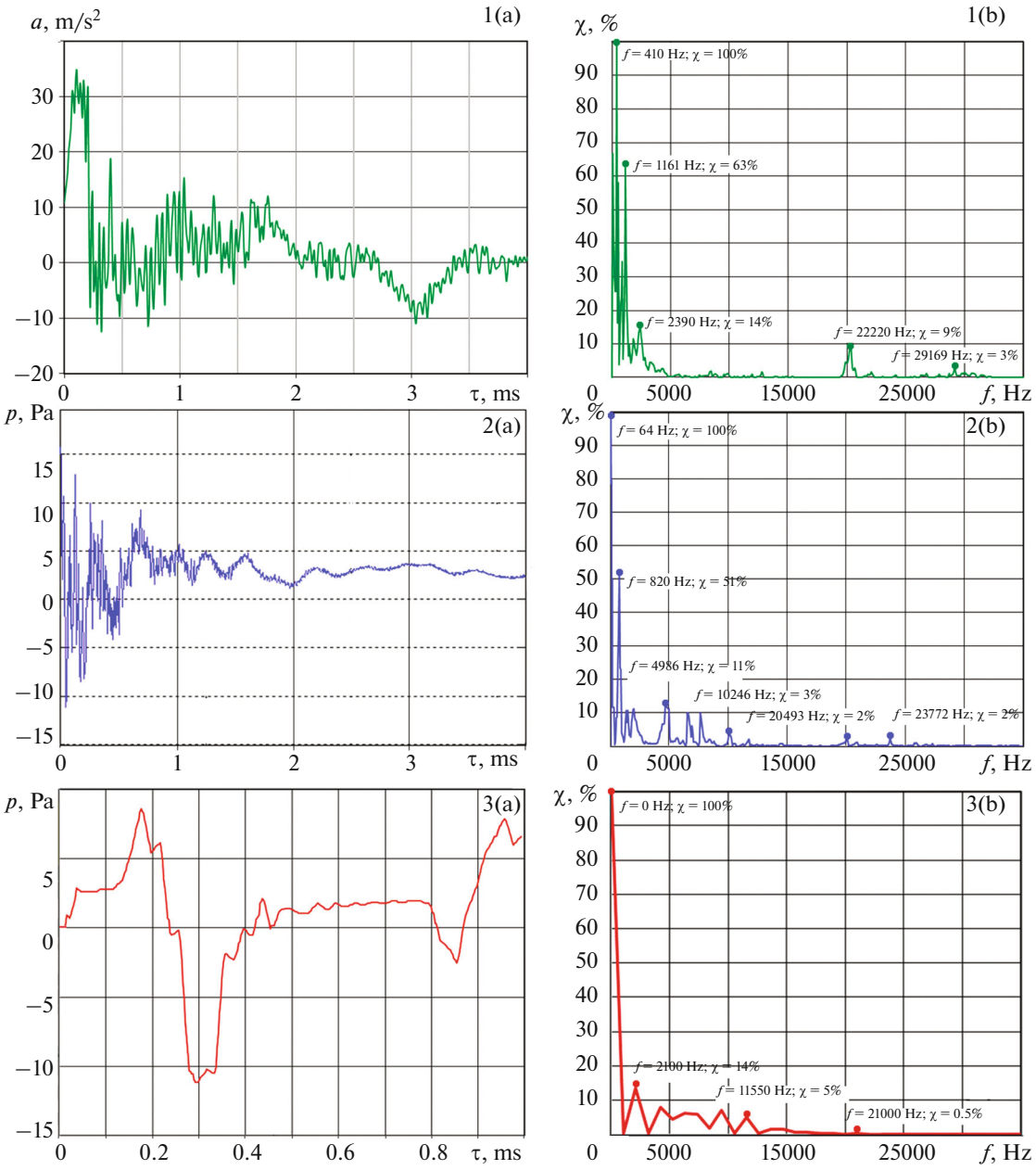

Fig. 10. Signal shapes (a, c, e) and frequency spectra (b, d, f) recorded by accelerometer (a, b), microphone (c, d) and obtained by numerical simulation (e, f) at the moment of Kevlar fiber breakage.

range recorded by the microphone and the accelerometer is primarily due to the measurement technique, as well as due to the difference in the modes of the recorded processes. The microphone was located in the acoustic chamber in the immediate vicinity of the fiber destruction zone (at a distance of 10–15 cm), whereas the accelerometer was installed at the end of the upper magnetic clamp approximately at the distance of half a meter from the breakage. The microphone recorded bulk waves, while the main modes for the accelerometer were longitudinal ones, which, accordingly, was reflected in the spectral characteristics of the energy density of the recorded signals.

Thus, the parameters of the pulses of recorded events and their waveforms and spectra depend on the characteristics and settings of the vibration analyzer used, wave processes recorded during the aftereffect of the fiber breakage, the frequency distribution of the released energy, and the degree of its dissipation.

CONCLUSIONS

According to the publications [8–15], only a small part of the energy released due to plastic deformation and rupture of metal samples (approximately 1%) is spent on acoustic emission. Figure 10 shows experimental and calculated results obtained when breaking a Kevlar fiber that confirm the validity of the above estimate. The peak partial energy values recorded in the ultrasonic frequency range during the aftereffect of the Kevlar fiber rupture ranged from 0.5 to 9% relative to the maximum level observed at frequencies $f = 0–500$ Hz.

The presented analysis of the propagation of elastic waves arising during deformation and breaking of bonds in the considered model of a solid body gives a general idea of the acoustic emission phenomenon, and of the transformation and dissipation of the energy released during the destruction of structural bonds in a solid. Acoustic emission is a very complex physical phenomenon reflecting the dynamic restructuring of bonds in the process of deformation of a solid body.

The interpretation of acoustic emission signals recorded by AE transducers in composite structures is especially difficult. This is due to not only the complex anisotropic structure of a multilayer PCM pack but also due to the fact that the process of damage accumulation and rupture of structural bonds at different scale levels in the layers with different fiber packing can occur both sequentially and in parallel, accompanied by a chain reaction in which different mechanisms of destruction come into action almost simultaneously [16–19]. In this case, pulses of elastic waves generated during the destruction of structural bonds in a multilayer PCM pack are significantly distorted during propagation as a result of velocity dispersion, interference of various wave modes, reverberation, and diffraction [20]. The indicated variety of influencing factors testifies to the complexity of identifying the nature of AE event sources in a multilayer complexly packed PCM and requires novel approaches to their recording and processing.

In recent years, several promising areas have been actively developing, among which one can distinguish, firstly, the data-kinetic concept of resource assessment [21–24], based on the hypothesis of the linear summation of damage and the stability of the critical value of the relative concentration of microcracks per unit of material volume. This concept has made it possible to predict the resource basing on concentration and kinetic parameters of AE diagnostics. Secondly, one should mention the structural–phenomenological approach. It uses the weight parameters of the content of AE event pulses in the energy clusters of the lower, middle, and upper levels [25, 26]; these parameters reflect the damage to the structure of the material at the micro-, meso-, and macroscale levels and allows one to assess the residual strength of the product in real time by comparing the current values of the criterion parameters with the limit ones, recorded at the moment of material destruction.

FUNDING

This work was supported by the Russian Science Foundation, project no. 20-19-00769.

REFERENCES

1. Ivanov, V.I. and Barat V.A., *Akustiko-emissionnaya diagnostika* (Acoustic-Emission Diagnostics), Moscow: Spektr, 2017.
2. Pollock, A., Acoustic emission testing, in *Metals Handbook,* Pollock, A., Ed., AST Int., 1989, vol. 17, pp. 278–294, 9th ed.
3. Makhutov, N.A., *Prochnost' i bezopasnost': fundamental'nye i prikladnye issledovaniya* (Strength and Safety: Basic and Applied Research), Novosibirsk: Nauka, 2008.

4. Matvienko, Yu.G., *Modeli i kriterii mekhaniki razrusheniya* (Fracture Mechanics Models and Criteria), Moscow: Fizmatlit, 2006.
5. Perel'muter, M.N., Growth criterion for cracks with bonds in the end region, *Prikl. Mat. Mekh.,* 2007, vol. 71, no. 1, pp. 152–171.
6. Hallquist, J.O., *LS-DYNA Theoretical Manual,* Livermore Software Technol. Corp., 2006.
7. *Kompozitsionnye materialy / Spravochnik* (Composite materials. Reference Book), Vasil'eva, V.V. and Tarnopol'skii, Yu.M., Eds., Moscow: Mashinostroenie, 1990.
8. Gillis, P.P. and Hamstad, M.A., Some fundamental aspect of the theory of the acoustic emission, *Mater. Sci. Eng.,* 1974, vol. 14, no. 1, pp. 103–108.
9. Baranov, V.M. and Molodtsov, K.I., *Akusticheskie pribory yadernoi energetiki* (Acoustic Devices for Nuclear Power), Moscow: Atomizdat, 1980.
10. Baranov, V.M., Kudryavtsev, E.M., Sarychev, G.A., and Shchavelin, V.M., *Akusticheskaya emissiya pri trenii* (Frictional Acoustic Emission), Moscow: Energoatomizdat, 1998.
11. Bigus, G.A., Daniev, Yu.F., Bystrova, N.A., and Galkin, D.I., *Osnovy diagnostiki tekhnicheskikh ustroistv i sooruzhenii* (Fundamentals of Diagnostics of Technical Devices and Structures), Moscow: Mosk. Gos. Tekh. Univ. im. N.E. Baumana, 2015.
12. Sjögren, T. and Svensson, I.L., Studying elastic deformation behaviour of cast irons by acoustic emission, *Int. J. Cast Metal Res.,* 2013, vol. 18, no. 4, pp. 249–56.
13. Pomponi, E. and Vinogradov, A., A real-time approach to acoustic emission clustering, *Mech. Syst. Signal Process.*, 2013, vol. 40, no. 2, pp. 791–804.
14. Pomponi, E., Vinogradov, A., and Danyuk, A., Wavelet based approach to signal activity detection and phase picking: Application to acoustic emission, *Signal Process,* 2015, vol. 115, pp. 110–119.
15. Kietov, V., Henschel, S., and Krüger, L., Study of dynamic crack formation in nodular cast iron using the acoustic emission technique, *Eng. Fract. Mech.,* 2018, vol. 188, no. 1, pp. 58–69.
16. Gresil, M., Saleh, M.N., Arshad, M., and Soutis, C., Defect quantification in 3D angle interlock glass fibre composites using acoustic emission, *8th Eur. Workshop Struct. Health Monit.* (EWSHM 2016) (Bilbao, Spain, July 5–8, 2016), pp. 1–10.
17. Hanuman, N.S.V.N. and Bose, T., Acoustic nondestructive evaluation of Glass-Fibre Reinforced Plastic (GFRP) plate, *NDE 2018 Conf. & Exhib. Soc. NDT (ISNT, NDE-India 2018)* (Mumbai, India, December 19–21, 2018), pp. 1–6.
18. Saeedifar, M., Najafabadi, M.A., Mohammadi, K., Fotouhi, M., Toudeshky, H.H., and Mohammadi, R., Acoustic emission-based methodology to evaluate delamination crack growth under quasi-static and fatigue loading conditions, *J. Nondestr. Eval.,* 2018, vol. 37, no. 1, pp. 1–13.
19. Sause, M.G.R., On use of signal features for acoustic emission source identification in fibre-reinforced composites, *33rd Eur. Conf. Acoust. Emission Test. (EWGAE)* (Senlis. France, September 12–14, 2018), pp. 1–12.
20. Matvienko, Yu.G., Vasil'ev, I.E., Bubnov, M.A., and Chernov, D.V., Influence of dimensions and shape of process cutouts on the accuracy of locating acoustic emission sources, *Russ. J. Nondestr. Test.,* 2020, vol. 56, no. 2, pp. 101–109.
21. Glebovsky, P.A. and Petrov, Yu.V., Kinetic interpretation of the structural-time criterion of fracture, *Solid State Phys.,* 2004, vol. 24, no. 6, pp. 1021–1024.
22. Nosov, V.V., Acoustic-emission quality control of plastically deformed blanks, *Russ. J. Nondestr. Test.,* 2017, vol. 53, no. 5, pp. 368–377.
23. Nosov, V.V. and Zelenskii, N.A., Estimating the strength of welded hull elements of a submersible based on the micromechanical model of temporal dependences of acoustic-emission parameters, *Russ. J. Nondestr. Test.,* 2017, vol. 53, no. 2, pp. 89–95.
24. Chernov, D.V., Algorithm for determining the onset of plastic deformation based on a micromechanical model of acoustic emission, *Vestn. Mosk. Energ. Inst.,* 2016, no. 3, pp. 97–103.
25. Matvienko, Yu.G., Vasil'ev, I.E., Chernov, D.V., and Elizarov, S.V., Criterion parameters for assessing degradation of composite materials by acoustic emission testing, *Russ. J. Nondestr. Test.,* 2018, vol. 54, no. 12, pp. 811–819.
26. Vasil'ev, I.E., Matvienko, Yu.G., Chernov, D.V., and Elizarov, S.V., Monitoring the accumulation of damage in the caisson of the stabilizer of the MS-21 airframe with the use of acoustic emission, *Probl. Mashinostr. Avtom.,* 2020, no. 2, pp. 118–141.